EUROPEAN ORGANIZATION FOR NUCLEAR RESEARCH

CERN-AB-2006-002

Intrabeam Scattering with Non-Ultrarelativistic Corrections and Vertical Dispersion for MAD-X

Frank Zimmermann, CERN, Geneva, Switzerland

Abstract

Using the Bjorken-Mtingwa recipe [1] we derive general formulae for the three intrabeam scattering (IBS) growth rates, including non-ultrarelativistic terms and vertical dispersion. These formulae have been implemented in the most recent version of MAD-X. An application to the LHC illustrates the effect of crossing angles and detector £elds on the vertical IBS growth rate. The increase of all three IBS growth rates for various LHC upgrade scenarios is also calculated. A third example, from the CLIC damping ring, demonstrates the importance of the spurious vertical dispersion generated by errors for the vertical IBS growth rate. Some limitations of this approach to intrabeam scattering are discussed.

Geneva, Switzerland

January 9, 2006

1 Introduction

The motivation for a revision of the MAD-X intrabeam scattering formulae is twofold.

First, CERN experiments at low or medium energy were reported to disagree with the MAD predictions [2]. As a mitigation, Michel Martini recommended the implementation of the Martini-Conte formulae [3], which are a non-ultrarelatvistic generalization based on the general Bjorken-Mtingwa formalism [1].

Second, neither the Bjorken-Mtingwa nor the Conte-Martini formulae account for nominal or spurious vertical dispersion, though the latter is thought to make the dominant contribution to the vertical IBS growth rate. Neglecting the vertical dispersion has given rise to peculiar results, such as predicting the shrinkage of the vertical emittance, which are not observed in reality. In linear collider damping rings, intrabeam scattering determines the £nal vertical emittance and when modelling the damping-ring performance it must properly be accounted for.

In this report we re-derive extended formulae for the emittance growth due to intrabeam scattering, following the general recipe of Bjorken and Mtingwa, and we con£rm the expressions for the longitudinal and vertical growth rate given by Conte and Martini, but we obtain a slightly different result for the horizontal plane. Next, we extend the formulae in a straightforward manner so as to include the effect of the vertical dispersion. Without vertical dispersion, the vertical growth rate is negligible and negative. Including even a tiny amount of vertical dispersion gives a non-negligible positive growth rate.

Inspection of the original MAD-X code revealed, unexpectedly, that the Conte-Martini formulae [3] were already implemented (presumably they had been copied from the ZAP code [4]), and not the original ones of Bjorken and Mtingwa [1]. We corrected these formulae for the horizontal plane and added the terms required for the vertical dispersion.

We note the existence of an alternative formalism of intrabeam scattering, developed earlier by Piwinski [5], as well as of a 'modi£ed' Piwinski formulation proposed by Bane [6], in which D_x^2/β is replaced by the dispersion invariant. Bane has also shown that in the limit of high beam energy the modi£ed Piwinski formalism gives the same results as the Bjorken-Mtingwa one. We have opted for the Bjorken-Mtingwa formalism as basis for calculating intrabeam scattering in MAD-X, since a different variant of this formalism had already been adopted for MAD-8 as well as for an earlier version of MAD-X.

2 Calculation Recipe

The derivation starts with expression (3.4) in [1] for the emittance growth rate in the direction d:

$$\frac{1}{\tau_d} = \frac{\pi^2 r_0^2 v_c m^3 N(\log)}{\gamma\Gamma} \left\langle \int_0^\infty \frac{d\lambda\ \lambda^{1/2}}{\left[\det\left(L+\lambda I\right)\right\}^{1/2}} \left\{ \mathrm{Tr} L^d\ \mathrm{Tr}\left(\frac{1}{L+\lambda I}\right) - 3\ \mathrm{Tr} L^d \left(\frac{1}{L+\lambda I}\right)\right\}\right\rangle\ , \tag{1}$$

where $d = x$, y, or l, r_0 is the classical particle radius, v_c the speed of light, m the particle mass, N the number of particles per bunch, $(\log) \equiv \ln\left(r_{\max}/r_{\min}\right)$ a Coulomb logarithm — with $r_{\max}$ denoting the smaller of σ_x and the Debye length and $r_{\min}$ the larger of the classical distance of closest approach and the quantum diffraction limit from the nuclear radius, typically assuming values of

$(\log) \approx 15 - 20$ —, γ the Lorentz factor, and, for a bunched beam, $\Gamma = (2\pi)^3(\beta\gamma)^3 m^3 \epsilon_x \epsilon_y \sigma_\delta \sigma_z$ the 6-dimensional invariant phase space volume of a bunched beam (corrected by a factor of $\sqrt{2}$ [7]) [1] ,

$$L = L^{(h)} + L^{(l)} + L^{(v)} \ , \tag{2}$$

with

$$L^{(h)} = \frac{\beta_x}{\epsilon_x} \begin{pmatrix} 1 & -\gamma\phi_x & 0 \\ -\gamma\phi_x & \gamma^2 H_x/\beta_x & 0 \\ 0 & 0 & 0 \end{pmatrix} \ , \tag{3}$$

$$L^{(l)} = \frac{\gamma^2}{\sigma_\delta^2} \begin{pmatrix} 0 & 0 & 0 \\ 0 & 1 & 0 \\ 0 & 0 & 0 \end{pmatrix} \ , \tag{4}$$

and, generalizing the Bjorken-Mtingwa theory to the case of nonzero vertical dispersion,

$$L^{(v)} = \frac{\beta_y}{\epsilon_y} \begin{pmatrix} 0 & 0 & 0 \\ 0 & \gamma^2 H_y/\beta_y & -\gamma\phi_y \\ 0 & -\gamma\phi_y & 1 \end{pmatrix} \ . \tag{5}$$

In the above expressions, $\phi_{x,y}$ and $H_{x,y}$ are de£ned as

$$\phi_{x,y} \equiv D'_{x,y} - \frac{\beta'_{x,y} D_{x,y}}{2\beta_{x,y}} \ , \tag{6}$$

and

$$H_{x,y} \equiv \frac{D_{x,y}^2 + \beta_{x,y}^2 \phi_{x,y}^2}{\beta_{x,y}} \ , \tag{7}$$

with $D_{x,y}$ the horizontal or vertical dispersion, $D'_{x,y}$ its slope, $\beta_{x,y}$ the beta function, and $\alpha_{x,y}$ the alpha Twiss function.

Bjorken and Mtingwa [1] proceeded by solving (1) with zero vertical dispersion, and neglecting β_x/ϵ_x and β_y/ϵ_y relative to $(\gamma D_x)^2/(\epsilon_x\beta_x)$, $(\beta_x/\epsilon_x)\gamma^2\phi_x^2$, and γ^2/σ_δ^2. Comte and Martini [3] kept the terms neglected by Bjorken and Mtingwa, which are important for $\gamma < 10$. We also keep the non-ultrarelativistic terms, and, in addition, we include the vertical dispersion.

3 IBS Growth Rates

For all three cases, namely Bjorken-Mtingwa, Conte-Martini, and the generalized expressions described in this report and now implemented in MAD-X, the three growth rates obtained from (1) can be written in the general form:

$$\frac{1}{\tau_x} \ = \ \frac{\pi^2 r_0^2 v_c m^3 N(\log)}{\gamma\Gamma} \left[\frac{\gamma^2 H_x}{\epsilon_x}\right] \int_0^\infty \frac{d\lambda \ \lambda^{1/2} \left[a_x\lambda + b_x\right]}{(\lambda^3 + a\lambda^2 + b\lambda + c)^{3/2}} \ ,$$

[1] For an unbunched beam, (1) also applies, if one uses $\Gamma = 4\pi^{5/2}(\beta\gamma)^3 m^3 \epsilon_x \epsilon_y \sigma_\delta C$, with C the ring circumference. In this case, Γ is equal to the 6-dimensional invariant phase space volume divided by $\sqrt{2}$.

$$\frac{1}{\tau_l} = \frac{\pi^2 r_0^2 v_c m^3 N(\log)}{\gamma\Gamma}\left[\frac{\gamma^2}{\sigma_\delta^2}\right]\int_0^\infty \frac{d\lambda\ \lambda^{1/2}\left[a_l\lambda + b_l\right]}{(\lambda^3 + a\lambda^2 + b\lambda + c)^{3/2}}\ ,$$
$$\frac{1}{\tau_y} = \frac{\pi^2 r_0^2 v_c m^3 N(\log)}{\gamma\Gamma}\left[\frac{\beta_y}{\epsilon_y}\right]\int_0^\infty \frac{d\lambda\ \lambda^{1/2}\left[a_y\lambda + b_y\right]}{(\lambda^3 + a\lambda^2 + b\lambda + c)^{3/2}}\ . \qquad (8)$$

The coef£cients a and b of the denominator are the same for all three planes. The eight coef£cients a, b, a_x, b_x, a_l, b_l, a_y, and b_y depend on the approximation. They are listed in Table 1 for all three approaches, i.e., Bjorken-Mtingwa's ultrarelativistic limit, the Conte-Martini formulae, and the expressions including vertical dispersion newly derived. In the limit of vanishing vertical dispersion, the latter reduce to the longitudinal and vertical IBS emittance growth rates of Conte and Martini [3]. However, the new expression for the horizontal growth rate differs in that two terms of Conte and Martini, one each for a_x and b_x — in Table 1 highlighted by bold face and curly brackets —, are absent in our re-derived theory. For the example applications which we present below the contribution from these two terms turns out to be negligible.

Table 1: Coef£cients for the IBS growth rate expressions, Eq. (8), in the three formalisms. In the limit of zero vertical dispersion, the right column reduces to the Conte-Martini expressions except for a_x and b_x, where the two terms in curly brackets and bold face are not reproduced.

	Bjorken-Mtingwa [1]	Conte-Martini [3]	this paper & new MAD-X
a	$\frac{\gamma^2 H_x}{\epsilon_x} + \frac{\gamma^2}{\sigma_\delta^2}$	$\frac{\gamma^2 H_x}{\epsilon_x} + \frac{\gamma^2}{\sigma_\delta^2} + \frac{\beta_x}{\epsilon_x} + \frac{\beta_y}{\epsilon_y}$	$\gamma^2\left(\frac{H_x}{\epsilon_x} + \frac{H_y}{\epsilon_y}\right) + \frac{\gamma^2}{\sigma_\delta^2} + \left(\frac{\beta_x}{\epsilon_x} + \frac{\beta_y}{\epsilon_y}\right)$
b	$\left(\frac{\beta_x}{\epsilon_x} + \frac{\beta_y}{\epsilon_y}\right)\left(\frac{\gamma^2 D_x^2}{\epsilon_x\beta_x} + \frac{\gamma^2}{\sigma_\delta^2}\right) + \frac{\beta_x\beta_y}{\epsilon_x\epsilon_y}\gamma^2\phi_x^2$	$\left(\frac{\beta_x}{\epsilon_x} + \frac{\beta_y}{\epsilon_y}\right)\left(\frac{\gamma^2 D_x^2}{\epsilon_x\beta_x} + \frac{\gamma^2}{\sigma_\delta^2}\right) + \frac{\beta_x\beta_y}{\epsilon_x\epsilon_y}\gamma^2\phi_x^2 + \frac{\beta_x\beta_y}{\epsilon_x\epsilon_y}$	$\left(\frac{\beta_x}{\epsilon_x} + \frac{\beta_y}{\epsilon_y}\right)\left(\frac{\gamma^2 D_x^2}{\epsilon_x\beta_x} + \frac{\gamma^2 D_y^2}{\epsilon_y\beta_y} + \frac{\gamma^2}{\sigma_\delta^2}\right) + \frac{\beta_x\beta_y}{\epsilon_x\epsilon_y}\gamma^2\left(\phi_x^2 + \phi_y^2\right) + \frac{\beta_x\beta_y}{\epsilon_x\epsilon_y}$
c	$\frac{\beta_x\beta_y}{\epsilon_x\epsilon_y}\left(\frac{\gamma^2 D_x^2}{\epsilon_x\beta_x} + \frac{\gamma^2}{\sigma_\delta^2}\right)$	$\frac{\beta_x\beta_y}{\epsilon_x\epsilon_y}\left(\frac{\gamma^2 D_x^2}{\epsilon_x\beta_x} + \frac{\gamma^2}{\sigma_\delta^2}\right)$	$\frac{\beta_x\beta_y}{\epsilon_x\epsilon_y}\left(\frac{\gamma^2 D_x^2}{\epsilon_x\beta_x} + \frac{\gamma^2 D_y^2}{\epsilon_y\beta_y} + \frac{\gamma^2}{\sigma_\delta^2}\right)$
a_x	$\frac{2\gamma^2 H_x}{\epsilon_x} + \frac{2\gamma^2}{\sigma_\delta^2}$	$\frac{2\gamma^2 H_x}{\epsilon_x} + \frac{2\gamma^2}{\sigma_\delta^2} - 2\frac{\beta_x}{\epsilon_x} - \frac{\beta_y}{\epsilon_y} + \frac{\beta_x}{\gamma^2 H_x}\left(\left\{\frac{\mathbf{6\beta_x}}{\epsilon_\mathbf{x}}\gamma^\mathbf{2}\phi_\mathbf{x}^\mathbf{2}\right\} - \frac{\gamma^2}{\sigma_\delta^2} + \frac{2\beta_x}{\epsilon_x} - \frac{\beta_y}{\epsilon_y}\right)$	$2\gamma^2\left(\frac{H_x}{\epsilon_x} + \frac{H_y}{\epsilon_y} + \frac{1}{\sigma_\delta^2}\right) - \frac{\beta_x H_y}{H_x\epsilon_y} + \frac{\beta_x}{H_x\gamma^2}\left(\frac{2\beta_x}{\epsilon_x} - \frac{\beta_y}{\epsilon_y} - \frac{\gamma^2}{\sigma_\delta^2}\right)$
b_x	$\left(\frac{\beta_x}{\epsilon_x} + \frac{\beta_y}{\epsilon_y}\right)\left(\frac{\gamma^2 D_x^2}{\epsilon_x\beta_x} + \frac{\gamma^2}{\sigma_\delta^2}\right) + \frac{\beta_x}{\epsilon_x}\frac{\beta_z}{\epsilon_z}\gamma^2\phi_x^2$	$\left(\frac{\beta_x}{\epsilon_x} + \frac{\beta_y}{\epsilon_y}\right)\left(\frac{\gamma^2 H_x}{\epsilon_x} + \frac{\gamma^2}{\sigma_\delta^2}\right) - \frac{\beta_x^2}{\epsilon_x^2}\gamma^2\phi_x^2 + \left(\frac{\beta_x}{\epsilon_x} - \frac{4\beta_y}{\epsilon_y}\right)\frac{\beta_x}{\epsilon_x} + \frac{\beta_x}{\gamma^2 H_x}\left(\frac{\gamma^2}{\sigma_\delta^2}\left(\frac{\beta_x}{\epsilon_x} - \frac{2\beta_y}{\epsilon_y}\right) + \left\{\frac{\mathbf{6\beta_x\beta_y}}{\epsilon_\mathbf{x}\epsilon_\mathbf{y}}\gamma^\mathbf{2}\phi_\mathbf{x}^\mathbf{2}\right\} + \frac{\beta_x\beta_y}{\epsilon_x\epsilon_y} - \gamma^2\frac{\beta_x^2\phi_x^2}{\epsilon_x^2}\right)$	$\left(\frac{\beta_x}{\epsilon_x} + \frac{\beta_y}{\epsilon_y}\right)\left(\frac{\gamma^2 H_x}{\epsilon_x} + \frac{\gamma^2 H_y}{\epsilon_x} + \frac{\gamma^2}{\sigma_\delta^2}\right) - \gamma^2\left(\frac{\beta_x^2}{\epsilon_x^2}\phi_x^2 + \frac{\beta_y^2}{\epsilon_y^2}\phi_y^2\right) + \left(\frac{\beta_x}{\epsilon_x} - \frac{4\beta_y}{\epsilon_y}\right)\frac{\beta_x}{\epsilon_x} + \frac{\beta_x}{\gamma^2 H_x}\left(\frac{\gamma^2}{\sigma_\delta^2}\left(\frac{\beta_x}{\epsilon_x} - \frac{2\beta_y}{\epsilon_y}\right) + \frac{\beta_x\beta_y}{\epsilon_x\epsilon_y} + \gamma^2\left(\frac{2\beta_y^2\phi_y^2}{\epsilon_y^2} - \frac{\beta_x^2\phi_x^2}{\epsilon_x^2}\right)\right) + \frac{\beta_x H_y}{\epsilon_y H_x}\left(\frac{\beta_x}{\epsilon_x} - \frac{2\beta_y}{\epsilon_y}\right)$
a_l	$2\gamma^2\left(\frac{H_x}{\epsilon_x} + \frac{1}{\sigma_\delta^2}\right)$	$2\gamma^2\left(\frac{H_x}{\epsilon_x} + \frac{1}{\sigma_\delta^2}\right) - \frac{\beta_x}{\epsilon_x} - \frac{\beta_y}{\epsilon_y}$	$2\gamma^2\left(\frac{H_x}{\epsilon_x} + \frac{H_y}{\epsilon_y} + \frac{1}{\sigma_\delta^2}\right) - \frac{\beta_x}{\epsilon_x} - \frac{\beta_y}{\epsilon_y}$
b_l	$\left(\frac{\beta_x}{\epsilon_x} + \frac{\beta_y}{\epsilon_y}\right)\left(\frac{\gamma^2 D_x^2}{\epsilon_x\beta_x} + \frac{\gamma^2}{\sigma_\delta^2}\right) + \frac{\beta_x\beta_y}{\epsilon_x\epsilon_y}\gamma^2\phi_x^2$	$\left(\frac{\beta_x}{\epsilon_x} + \frac{\beta_y}{\epsilon_y}\right)\left(\frac{\gamma^2 D_x^2}{\epsilon_x\beta_x} + \frac{\gamma^2}{\sigma_\delta^2}\right) + \frac{\beta_x\beta_y}{\epsilon_x\epsilon_y}\gamma^2\phi_x^2 - \frac{2\beta_x\beta_y}{\epsilon_x\epsilon_y}$	$\left(\frac{\beta_x}{\epsilon_x} + \frac{\beta_y}{\epsilon_y}\right)\gamma^2\left(\frac{H_x}{\epsilon_x} + \frac{H_y}{\epsilon_y} + \frac{1}{\sigma_\delta^2}\right) - 2\frac{\beta_x\beta_y}{\epsilon_x\epsilon_y} - \gamma^2\left(\frac{\beta_x^2\phi_x^2}{\epsilon_x^2} + \frac{\beta_y^2\phi_y^2}{\epsilon_y^2}\right)$
a_y	$-\frac{\gamma^2 H_x}{\epsilon_x} - \frac{\gamma^2}{\sigma_\delta^2}$	$-\gamma^2\left(\frac{H_x}{\epsilon_x} + \frac{\gamma^2}{\sigma_\delta^2} + \frac{\beta_x}{\epsilon_x} - \frac{2\beta_y}{\epsilon_y}\right)$	$-\gamma^2\left(\frac{H_x}{\epsilon_x} + \frac{2H_y}{\epsilon_y} + \frac{\beta_x}{\beta_y}\frac{H_y}{\epsilon_x} + \frac{1}{\sigma_\delta^2}\right) + 2\gamma^4\frac{H_y}{\beta_y}\left(\frac{H_y}{\epsilon_y} + \frac{H_x}{\epsilon_x}\right) + \frac{2\gamma^4 H_y}{\beta_y\sigma_\delta^2} - \left(\frac{\beta_x}{\epsilon_x} - \frac{2\beta_y}{\epsilon_y}\right)$
b_y	$\left(\frac{\beta_x}{\epsilon_x} + \frac{\beta_y}{\epsilon_y}\right)\left(\frac{\gamma^2 D_x^2}{\epsilon_x\beta_x} + \frac{\gamma^2}{\sigma_\delta^2}\right) + \frac{\beta_x\beta_y}{\epsilon_x\epsilon_y}\gamma^2\phi_x^2 - \frac{3\beta_x}{\epsilon_x}\left(\frac{\gamma^2 D_x^2}{\epsilon_x\beta_x} + \frac{\gamma^2}{\sigma_\delta^2}\right)$	$\left(\frac{\beta_x}{\epsilon_x} + \frac{\beta_y}{\epsilon_y}\right)\left(\frac{\gamma^2 D_x^2}{\epsilon_x\beta_x} + \frac{\gamma^2}{\sigma_\delta^2}\right) + \frac{\beta_x\beta_y}{\epsilon_x\epsilon_y}\gamma^2\phi_x^2 + \frac{\beta_x\beta_y}{\epsilon_x\epsilon_y} - \frac{3\beta_x}{\epsilon_x}\left(\frac{\gamma^2 D_x^2}{\epsilon_x\beta_x} + \frac{\gamma^2}{\sigma_\delta^2}\right)$	$\gamma^2\left(\frac{\beta_y}{\epsilon_y} - \frac{2\beta_x}{\epsilon_x}\right)\left(\frac{H_x}{\epsilon_x} + \frac{1}{\sigma_\delta^2}\right) + \left(\frac{\beta_y}{\epsilon_y} - \frac{4\beta_x}{\epsilon_x}\right)\frac{\gamma^2 H_y}{\epsilon_y} + \frac{\beta_x\beta_y}{\epsilon_x\epsilon_y} + \gamma^2\left(\frac{2\beta_x^2\phi_x^2}{\epsilon_x^2} - \frac{\beta_y^2\phi_y^2}{\epsilon_y^2}\right) + \frac{\gamma^4 H_y}{\beta_y}\left(\frac{\beta_x}{\epsilon_x} + \frac{\beta_y}{\epsilon_y}\right)\left(\frac{H_y}{\epsilon_y} + \frac{1}{\sigma_\delta^2}\right) + \left(\frac{\beta_y}{\epsilon_y} + \frac{\beta_x}{\epsilon_x}\right)\gamma^4\frac{H_x H_y}{\beta_y\epsilon_x} - \gamma^4\frac{H_y}{\beta_y}\left(\frac{\beta_x^2}{\epsilon_x^2}\phi_x^2 + \frac{\beta_y^2}{\epsilon_y^2}\phi_y^2\right)$

4 First Example: LHC

In the LHC, vertical dispersion is generated by the crossing angles at IP1 and IP2, and by the detector £elds of ALICE and LHC-b plus correction bumps. The peak vertical dispersion in the arcs is close to 0.2 m. Figures 1 and 2 show the nominal LHC dispersion at top energy. Table 2 lists IBS growth rates computed by a previous MAD-X version, which implemented the Conte-Martini formulae, and those by the new MAD-X version, which includes vertical dispersion. In the cases with crossing angles and detector £elds, there is a large difference in the vertical growth rate between the two MAD-X versions. Namely, the vertical growth time changes from -2.9×10^6 h (damping) for the old version of MAD to $+436$ h for the modi£ed MAD-X routine where the effect of vertical dispersion is taken into account. Figure 3 shows the local vertical IBS growth rate around the ring circumference, computed by the new MAD-X version for the LHC with crossing angles and detector £elds. The highest growth rates are found in the interaction regions 1 and 5.

Table 2: LHC IBS growth rates at 7 TeV computed with the old and new versions of MAD-X with and without crossing angles & LHCB/ALICE detector £elds. The full crossing angle in IP1 and IP5 is 285 μrad.

	without crossing angles & detector £elds		with crossing angles & detector £elds	
	old MAD-X	new MAD-X	old MAD-X	new MAD-X
τ_l [h]	57.5	57.5	57.5	58.6
τ_x [h]	103.3	103.3	102.5	104.2
τ_y [h]	-2.9×10^6	-2.9×10^6	-2.9×10^6	436.1

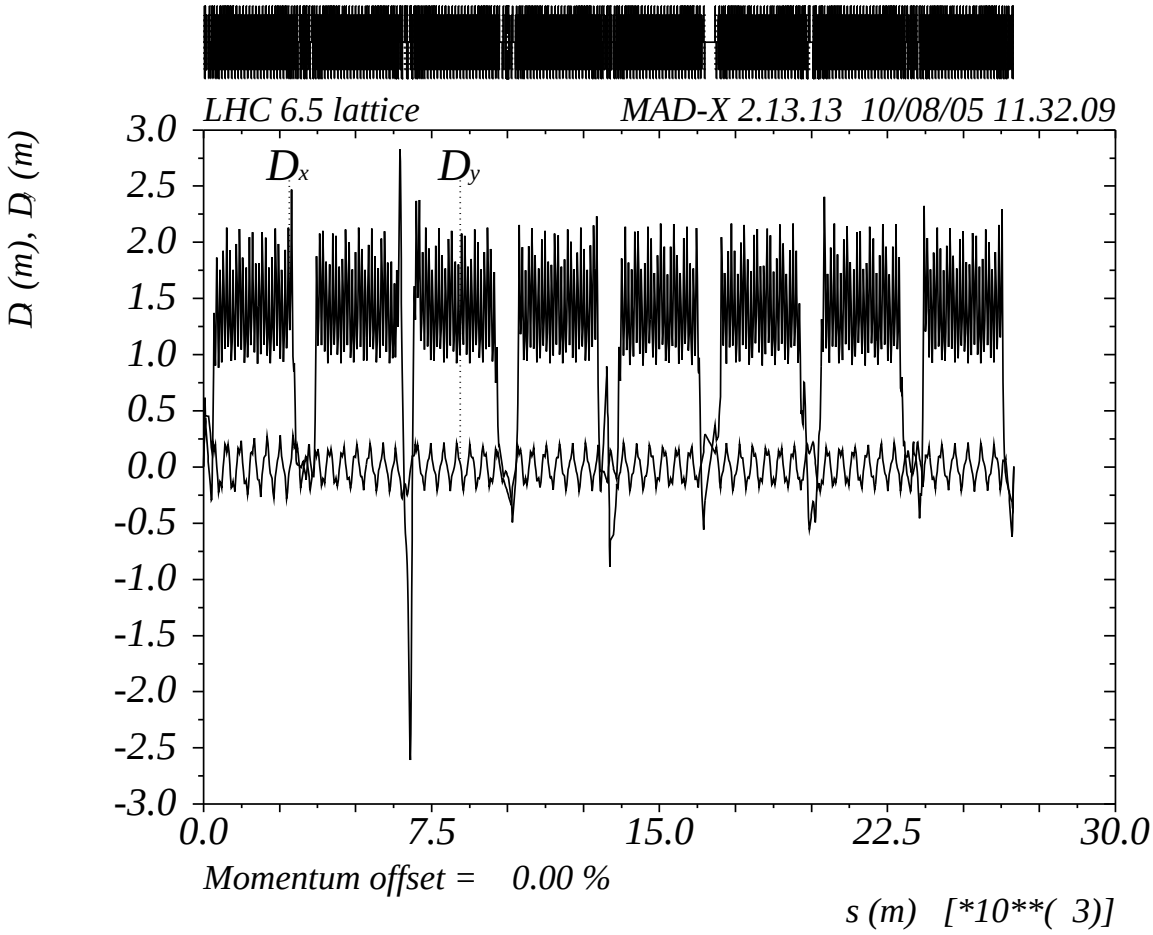

Figure 1: The horizontal and vertical dispersion functions in the LHC at top energy, with nominal crossing angles and zero separation at IP1, IP2, IP5 and IP8, and the ALICE and LHCB detector £elds turned on.

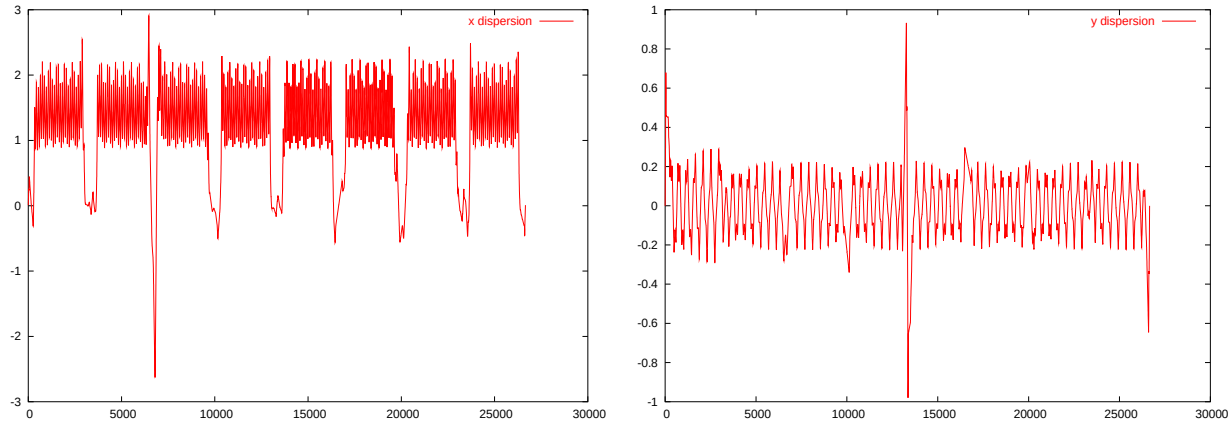

Figure 2: The horizontal (left) and vertical dispersion (right) in units of metre as a function of the position in metre, for the LHC at top energy, with nominal crossing angles and zero separation at IP1, IP2, IP5 and IP8, and the ALICE and LHCB detector £elds turned on.

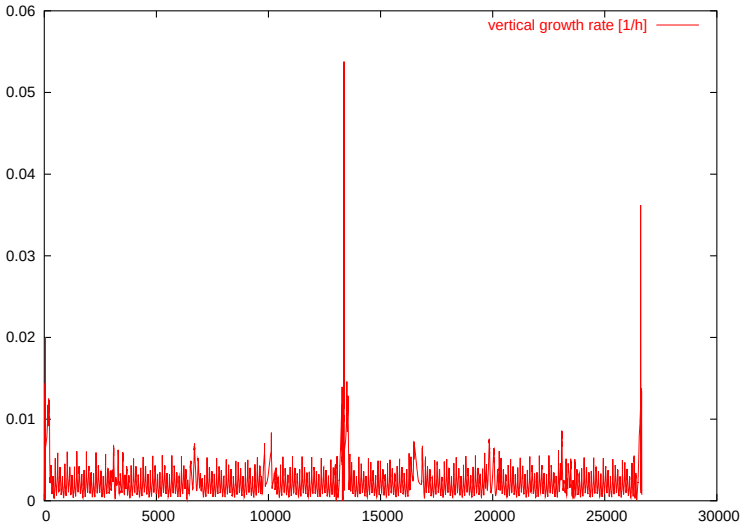

Figure 3: Local vertical IBS growth rate in units of 1/h as a function of position in m around the ring, for the LHC at top energy, with nominal crossing angles at IP1, IP2, IP5 and IP8, zero separation, and the ALICE and LHCB detector £elds turned on.

5 Second Example: LHC Upgrade

Upgrades of the LHC are being considered which increase the peak luminosity by a factor of ten to 10^{35} cm^{-2}s^{-1}. Various upgrade scenarios exist, which, e.g., foresee an increased bunch charge, larger crossing angles, smaller longitudinal emittances, and higher rf voltages or higher rf frequencies. The IBS growth rates tend to get signi£cantly larger in many of the scenarios considered. In case the injection energy into the LHC can be raised by new injectors ("SuperSPS"), a larger transverse normalized emittance may be accepted, which would allowing keeping a constant brightness $N_b/(\gamma\epsilon_{x,y})$ at higher bunch intensity. Table 3 lists IBS growth rates calculated with the new version of MAD-X for different upgrade options and parameter combinations. The second case illustrates that for increasing crossing angles the vertical growth rate soon becomes comparable to the horizontal one.

Table 3: LHC IBS growth rates computed with the new version of MAD-X for the nominal LHC and for various LHC upgrade scenarios. All cases refer to a beam energy of 7 TeV, and include crossing angles as well as LHCB/ALICE detector £elds. If not noted otherwise, the nominal LHC parameters are assumed, namely a bunch population of $N_b = 1.15 \times 10^{11}$, a transverse normalized emittance of $\gamma\epsilon_{x,y} = 3.75$ μm, an rms bunch length $\sigma_z = 7.55$ cm, an rms energy spread $\sigma_\delta = 1.129 \times 10^{-4}$, a longitudinal emittance $\epsilon_{||} = 2.5$ eVs, an rf voltage $V_{rf} = 16$ MV at 400 MHz, and full crossing angles of $\theta_c = 285$ μrad in IP1 and IP5.

case	τ_l [h]	τ_x [h]	τ_y [h]
nominal	58.6	104.2	436.
$N_b = 1.7 \times 10^{11}$, $\epsilon_{||} = 1.75$ eVs, $\sigma_z = 3.8$ cm, $\sigma_\delta = 1.55 \times 10^{-4}$, $V_{rf} = 120$ MV, $\theta_c = 445$ μrad	46.4	42.5	77.3
$N_b = 2.3 \times 10^{11}$, other values nominal	29.2	51.9	217.5
$N_b = 2.3 \times 10^{11}$, $\gamma\epsilon_{x,y} = 7.5$ μm	72.5	254.2	1075
$N_b = 2.3 \times 10^{11}$, $\epsilon_{||} = 1.25$ eVs, $\sigma_z = 5.2$ cm, $\sigma_\delta = 7.86 \times 10^{-5}$	9.3	32.8	138.3
$N_b = 2.3 \times 10^{11}$, $\epsilon_{||} = 1.25$ eVs, $\sigma_z = 3.7$ cm, $\sigma_\delta = 1.11 \times 10^{-4}$, $V_{rf} = 64$ MV	14.6	26.0	108.6

6 Third Example: CLIC Damping Ring

Intrabeam scattering is the dominant effect determining the equilibrium emittance in the CLIC damping ring [8]. Field errors creating vertical dispersion have a profound impact on the estimated vertical growth rate, and, therefore, on the equilibrium emittance. As an illustration, Fig. 4 presents the horizontal and vertical dispersion functions around the CLIC damping ring obtained with random tilt angles of all quadrupole magnets, described by a Gaussian distribution of $\sigma_\phi = 200$ μrad

standard deviation with a cut-off at $3\sigma_\phi$. One can recognize the two arcs and the two long straight wiggler sections. Table 4 compares the IBS growth rates computed by the old version of MAD-X, using the Conte-Martini formalism, and those from the new version of the code. While in the case of the ideal optics, there is no difference, the vertical growth time becomes a factor 6 shorter, when errors generating vertical dispersion are included. Figure 5 presents the local IBS growth rates as a function of position around the ring, for the case with errors.

This example underlines that in tuning studies for the CLIC damping ring, the dependence of the IBS growth rate on the residual vertical dispersion must be taken into account.

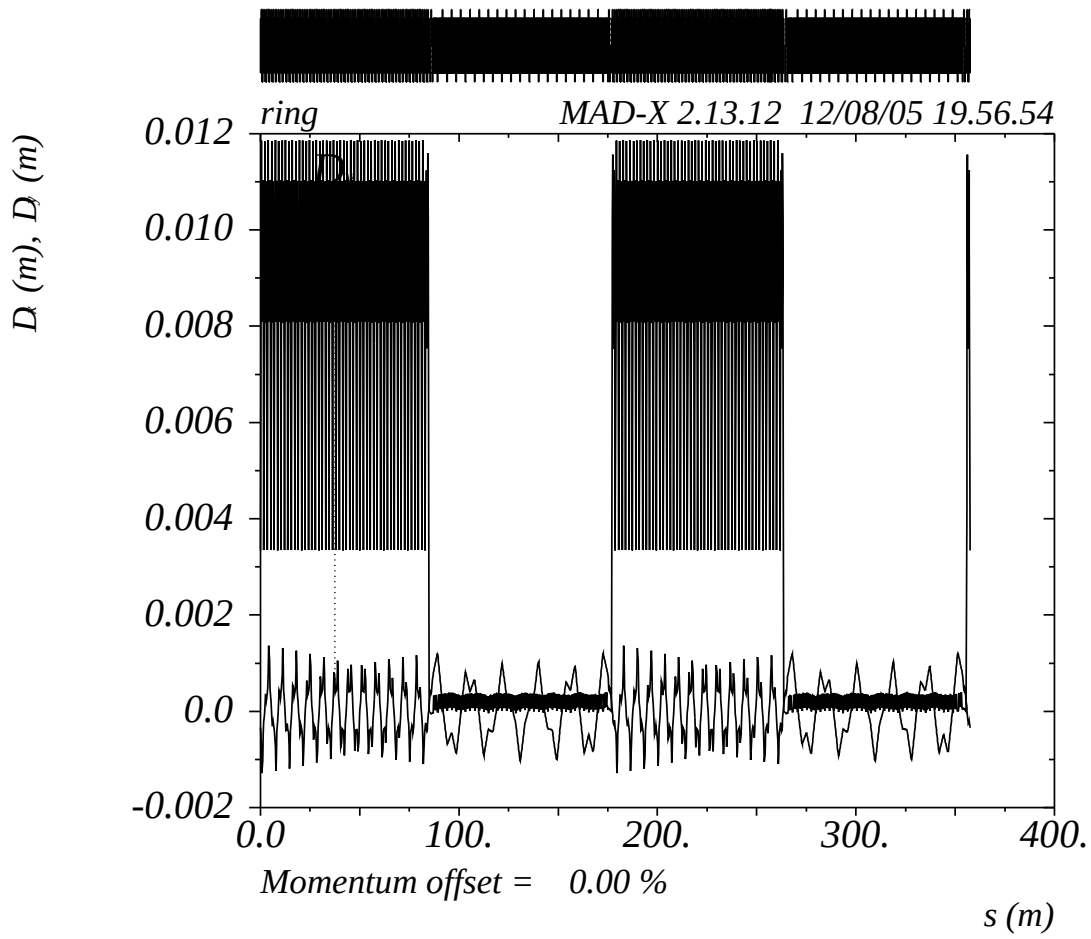

Figure 4: The horizontal and vertical dispersion functions in the CLIC damping ring with quadrupole random tilt angles of $\sigma_\phi = 200$ μrad cut off at $3\sigma_\phi$.

Table 4: IBS growth rates in the CLIC damping ring computed with the old and new version of MAD-X for the ideal optics and with random quadrupole roll angles of $\sigma = 200$ μrad, with a Gaussian distribution cut at 2.5 σ.

	no errors		errors	
	old MAD-X	new MAD-X	old MAD-X	new MAD-X
τ_l [ms]	2.2	2.2	2.2	2.2
τ_x [ms]	2.2	2.2	2.2	2.1
τ_y [ms]	12.6	12.6	12.6	2.0

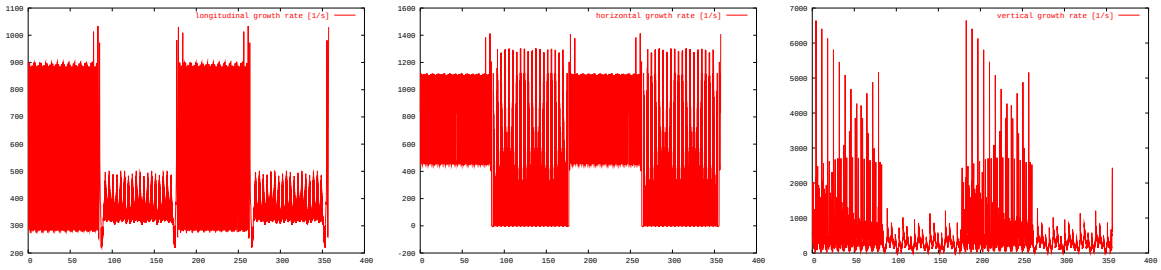

Figure 5: Local longitudinal, horizontal and vertical IBS growth rate in units of 1/s as a function of position in m around the CLIC damping ring, with quadrupole random tilt angles of $\sigma_\phi = 200$ μrad cut off at $3\sigma_\phi$.

7 Limitations and Outlook

The theory of Bjorken-Mtingwa calculates the rms emittance growth rates assuming Gaussian beams. In reality, a beam will not be exactly of Gaussian shape, e.g., due to the very effect of intrabeam scattering. The existing theories of Bjorken-Mtingwa or Piwinski do not predict the emittance growth for non-Gaussian distributions, neither do they describe the tails generated by intrabeam scattering.

An attempt to more correctly estimate the emittance growth of the beam core due to intrabeam scattering for electron or positron storage rings was proposed by Raubenheimer [9], who adjusted the upper limit of the Coulomb integral so as to discard single-scattering events over a radiation damping time, thereby removing the contribution of the tail increase to the rms growth rate. This modi£cation reduces the effective growth rate by about a factor of 0.6, compared with the conventional calculation.

An alternative and more comprehensive approach to address and to model tails are multi-particle Monte-Carlo simulations ála MOCAC [10], which is based on a binary collision model [11]. This type of code can model any distribution, but long computing times are implied. We consider adding a Monte-Carlo simulation IBS module to MAD-X in the longer-term future.

Coupling between the horizontal and vertical betatron motion is not accounted for in the formalism presented here.

Lastly, both the Bjorken-Mtingwa paper and our derivation in this paper start from an invariant Coulomb scattering amplitude of the form $M = 4\pi\alpha/q^2$, where α denotes the £ne-structure constant and q the four-momentum transfer. This scattering amplitude describes the Coulomb interaction of two charged spinless and point-like particles, with all the entailed limitations.

8 Summary

Applying the Bjorken-Mtingwa recipe, we have derived generalized expressions for the three intrabeam scattering growth rates, which are valid also if the beam energy is not ultrarelativistic, or if vertical dispersion is present either by design or due to errors. In the limit of zero vertical dispersion our result almost reduces to that of Conte and Martini, except for a small difference in the horizontal growth rate. Three examples, from the LHC, the LHC upgrade, and the CLIC damping ring, respectively, demonstrate that the effect of the vertical dispersion is predominant for the vertical growth rate, which is changed, for the LHC, by four orders of magnitude and in the sign, and, for the CLIC damping ring with errors, by a factor of 6. The new IBS formulae have been committed to the MAD-X code.

Acknowledgements

I thank A. Bolshakov, O. Brüning, J. Jowett, M. Martini, and A. Smirnov for helpful discussions, M. Korostelev for providing the optics of the CLIC damping ring, and A. Lehrach for re-emphasizing the importance of non-Gaussian distributions at the 2005 MAD-X day. In particular, I am grateful to F. Schmidt for encouraging this study and for his strong support.

References

[1] J.D. Bjorken, S.K. Mtingwa, “Intrabeam Scattering,” Part. Acc. Vol. 13, pp. 115–143 (1983).

[2] J.Y. Hemery, unpublished; private communication by M. Martini (2005).

[3] M. Conte, M. Martini, “Intrabeam Scatering in the CERN Antiproton Accumulator,” Part. Acc. Vol. 17, pp. 1–10 (1985).

[4] M. Zisman, S. Chattopadhyay, J. Bisognano, ZAP User’s Manual, LBL-21270, ESG-15 (1986).

[5] A. Piwinski, “Intrabeam Scattering,” Proc. Ninth Int. Conference on high Energy Accelerators, Stanford, Spring£eld, pp. 405–409 (1975).

[6] K.L.F. Bane, “A Simpli£ed Model of Intrabeam Scattering,” EPAC’02 Paris (2002).

[7] K. Kubo, K. Oide, “Intrabeam Scattering in Electron Storage Rings,” PRST-AB 4, 124401 (2001).

[8] M. Korostelev, F. Zimmermann, “A Lattice Design for the CLIC Damping Ring,” Nanobeam 2002, CERN-AB-2003-007 (ABP), and CLIC Note 558 (2002).

[9] T. Raubenheimer, “The Core Emittance with Intrabeam Scattering in e+/e- Storage Rings,” Part. Acc. 45, 111 (1994).

[10] P. Zenkevich, A. Bolshakov, O. Boine-Frankenheim, “Kinetic Effects in Multiple Intra-Beam Scattering,” ICFA HB204, Bensheim, AIP Conf. Proc. 773, 425 (2005).

[11] T. Takizuka and H. Abe, “A Binary Collision Model for Plasma Simulation with a Particle Code,” J. Comp. Physics 25, pp. 205–219 (1977).